IJISET - International Journal of Innovative Science, Engineering & Technology, Vol. 7 Issue 10, October 2020
ISSN (Online) 2348 – 7968 | Impact Factor (2020) – 6.72
www.ijiset.com

Hydrothermal Synthesis, Characterization and Gas Sensitivity of Nb_2O_5

Dr. S. V. Jagtap[1], S. D. Thakre[2], A. S. Tale[3] and S .B. Deshmukh[4]

[1] Department of Physics, R.D.I.K & K.D.College, Badnera (Rly), Amravati, Maharashtra, India

[2] Department of Physics, Dr. Rajendra Gode Institute of Technology & Research, Amravati, Maharashtra, India

[3] Department of Physics, Sant Gajanan Maharaj College of Engineering, Shegaon, Maharashtra, India

[4] Department of Chemistry, Smt. ACS College, Kiran Nagar, Amravati, Maharashtra, India

Abstract

Nanocrystalline Nb_2O_5 based thin film sensors of smaller crystallite size were prepared by modified hydrothermal method. The samples were characterized by X-ray diffraction, XPS, SEM and TEM analysis. The gas sensing performance of Nb_2O_5 sensors was demonstrated for the gases like acetone, ammonia and LPG. It was found that, Nb-450 thin films show the fast and optimum response towards 400 ppm ammonia gas at 250˚C. For the recovery process, the sample indicated slow recovery performance under most sensing situations. However, a comparatively better performance is observed over most of the reported Nb_2O_5 based sensors. These results provide new insights into the capabilities and limitations of Nb_20_5 sensors.

Keywords: ***Nb_2O: Niobium Oxide: Gas Sensor: H_2S Sensors:***

1. Introduction

Niobium Pentoxide (Nb_2O_5) is an n-type semiconductor with a band gap of about 3.4 eV, low in comparison to other oxides. The interest in studying the Nb_2O_5 is due to its remarkable physicochemical properties and structural isotropy suitable for a wide range of applications in the construction of gas sensing, electrochromics display and photoelectrodes, as well as in field-emission displays and microelectronics [1-6]. Studies were conducted in the past on the use of Nb_2O_5 nanoparticles for environmental remediation in water through of photocatalytic processes because of its stability in an aqueous medium, its surface acidity, redox and photocatalytic properties, which are intrinsically linked to its structure [7-9]. Band gap of Nb_2O_5 has been reported to vary from semiconducting (3.1 eV) to insulating (5.3 eV) range and can be adjusted through doping, changes in crystallinity and stoichiometry and heat treatment to obtain different phases. The most stable phases of Nb_2O_5 are the orthorhombic (*o*), tetragonal (*t*) and monoclinic (*m*), usually activated *via* thermal treatment at 800, 1000 and 1100˚C respectively with typically an amorphous polymorphs below 500˚C.

Sensor devices based on Nb_2O_5 for gas, humidity, biological and chemical sensing as well as photodetection have been successfully demonstrated. Generally, the main parameters for good sensing device performance are the size, morphology, aspect ratio, intergranular connectivity, porosity, surface energy, stoichiometry and surface area to volume ratio of the incorporated sensing material [10, 11]. Depending on the type of gas species, reducing or oxidizing, the interaction between the gas molecules and the Nb_2O_5 films changes the charge carrier concentration and the potential barrier of the Nb_2O_5 films. These affect the physio-chemical property of the films corresponding to the gas constituents exposed to the sensor. So far, the investigated gases that have been examined using Nb_2O_5 are O_2, hydrogen (H_2), dissolved O_2, carbon monoxide (CO), ammonia (NH_3) and a number of hydrocarbons (HCs) [12-24]. The detection principle of this material is based on the reversible modulation of the electrical conductance in the presence of oxidizing or reducing gases.

In this research, Nb_2O_5 nanosize powders were prepared by modified hydrothermal method using different sintering temperatures (400-550°C). The powders obtained were characterized by X-ray diffraction (XRD), scanning electron microscopy (SEM) and Transmission electron microscopy (TEM). Also by the BET method in order to obtain measurements of surface area, the UV-vis diffuse reflectance spectroscopy (DRS) to identify the band gap energy and the Raman spectroscopy to perform a vibrational characterization.

2 Experimental Details

2.1 Synthesis of Nb_2O_5 Powders

Niobium pentachloride ($NbCl_5$), Liquid ammonia (NH_3), Potassium permanganate ($KMnO_4$), Sodium nitrate ($NaNO_3$) and hydrogen peroxide (H_2O_2) were purchased from Merck Chemicals. Double distilled water was used throughout the synthesis procedure. All chemicals were used as received without any further purification.

In a typical synthesis, 5 g Niobium pentachloride was mixed with 20% ammonia solution and 20% H_2O_2 to give a sol. To the sol, the mixture of 1 M Ethylene glycol and 0.2 M NaOH solution was added and the mixture was stirred for 1 h at 50˚C. The prepared solution was transferred into a Teflon-lined stainless steel autoclave of 100 mL capacity and sealed. The reaction was performed at 300˚C for 10 h followed by the cooling to room temperature. Further, the obtained white precipitate was centrifuged for the separation of the powder from liquid. It was then washed 3-4 times with deionized water and ethanol and dried at 50˚C for 4 h in air. Finally, the Nb_2O_5 modified materials were obtained by the calcination of obtained precipitate in air atmosphere at 400, 450, 500 and 550˚C for 4 h and samples were coded as Nb-400, Nb-450, Nb-500 and Nb-550 respectively.

2.2 Preparation of Nb_2O_5 Thin Films

For the screen printing technique, the paste of as synthesized Nb_2O_5 powder was prepared by dissolving it in appropriate quantity of terpineol. Further, the paste was screened on the glass substrate with the dimension of 8 x 12 mm^2, and then the films were dried and heated in a box furnace in the air at the temperature of 500˚C for 30 min. The films obtained were then examined to study their physical and gas sensing properties.

2.3 Characterization

Crystal structures of the commercial and synthesized Nb_2O_5 samples were studied by XPS and X-ray diffraction (XRD) techniques. Powder XRD patterns were recorded on a Philips diffractometer (PW1800, CuKα radiation, graphite monochromator). Particle shape and product morphology were characterized by scanning electron microscope. Measurements of the surface area of the dry powder were done by nitrogen adsorption–desorption isothermal analysis. Mean diameter of particles was determined by counting the particles shown in TEM images.

3. Results and Discussion

3.1 X-ray Diffraction Analysis

Figure 3.1 *XRD* patterns peak analysis verifies that those Nb_2O_5 samples obtained by the modified hydrothermal method heated at 450°C have the orthorhombic crystalline structure due to the existence of dominant diffraction peaks according to PDF cards No. 30-0873 (contained in the Power Diffraction File) for the T-Nb_2O_5 phase, (a = 6.168 Å, b = 29.312 Å, c = 3.936Å). The *XRD* patterns of the samples calcined at 400°C also displayed the existence of the T-Nb_2O_5 phase although with less crystallinity.

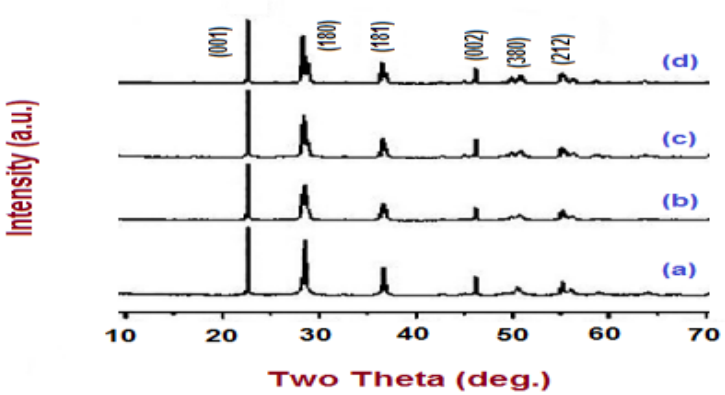

Figure 3.1 XRD pattern of as synthesized Nb_2O_5 samples calcined at (a) 400˚C, (b) 450˚C, (c) 500˚C and (d) 550˚C.

To analyze the crystallite growth, the crystallite size (d) of the Nb_2O_5 nanoparticles was calculated by the Scherrer's equation:

$$d = \frac{K\lambda}{\beta cos\theta}$$

where, K is the shape correction factor, the value 0.9 is taken as the volume-averaged crystallite dimension perpendicular to the *hkl* diffraction plane; λ is the wavelength used, θ is the Bragg diffraction angle measured *hkl* peak and β represents the *FWHM* (Full width at half maximum) measured in radians on the 2θ scale [22]. The broadening lines chosen for the *d* estimate correspond to (001), (180), (181), (002), (380), and (212) crystalline planes according to PDF No. 01-071-0336 reported in Inorganic Crystal Structure Database (ICSD) [23]. The crystallite size of nanoparticles on the T-Nb_2O_5 phase increases in the range of 20 to 50 nm with an increase in calcination temperature, as shown Table 3.1.

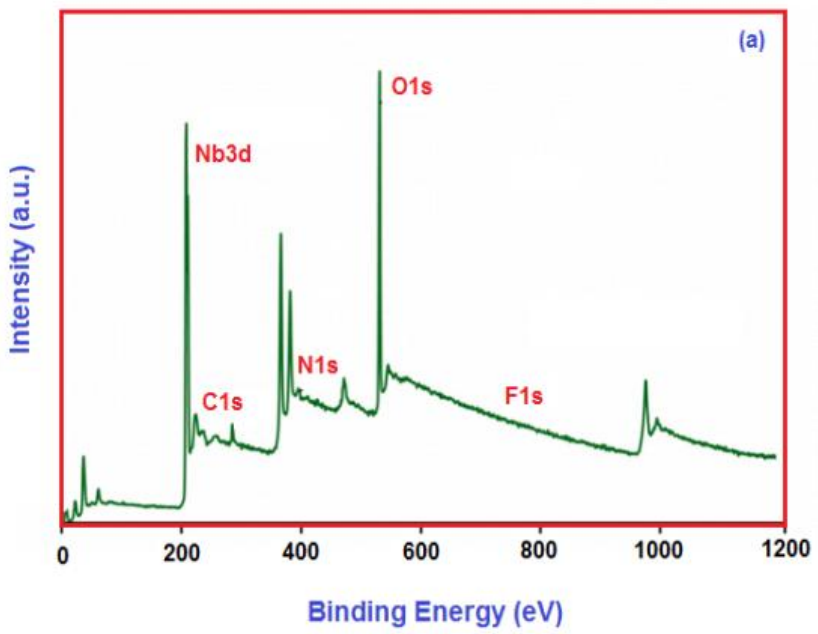

Figure 3.2(a) The XPS scan of the Nb_2O_5 calcined at 450˚C.

Table 3.1 Calcination temperature, crystallite size (obtained from (001) & (180) planes of XRD) and specific surface area of as synthesized Nb_2O_5 samples.

Samples	Calcination Temperature (˚C)	Crystallite Size (nm)		Specific Surface Area (S_{BET})
		(001)	(180)	(m^2/g)
Nb-400	400	36.3	37.6	11.54
Nb-450	450	11.7	12.6	75.42
Nb-500	500	22.5	24.3	22.14
Nb-550	550	35.6	36.3	13.23

Table 3.1 also shows the results of specific surface area, S_{BET} determined by taking data at relative pressures between 0.02 and 0.15. The method had accuracy constraints during the measurement process. This fact was observed because the values of S_{BET} were less than $10m^2$/g. The S_{BET} data show that the increase in the calcination temperature from 450°C to 550°C resulted in the progressive decrease of specific surface area of the Nb_2O_5 nanosized powders. This is mainly because a more high calcination temperature can lead to a greater proportion of the pore coalescence due to the further crystallization of walls separating mesopores in their structure which be established through measurement of pore size.

3.2 XPS Analysis

An XPS analysis was employed to determine the chemical com-position and valencies of the Nb_2O_5. Figure 3.2(a) shows the spectrum of the Nb2O5 sample calcined at 450˚C. The signals of Nb and O are visible, confirming the

presence of niobium and oxygen elements. As shown in Figure 3.2(b), the high-resolution spectrum for the Nb region exhibits the $Nb3d_{3/2}$ peak at 210.08 eV and $Nb3d_{5/2}$ at 207.28 eV. The spectra obtained indicate that the film is composed of Nb_2O_5, which is consistent with a previous report [**43**]. The existence of low peak of C1s in the survey spectrum is expected due to CO_2 adsorption or contamination carbon from the environment. Unlike other metal oxides such as anodized TiO_2 [**44**], the XPS pattern shows that there is no fluoride doping effect after the anodization process, which is beneficial for reducing the internal electron scattering during the passage of electrical current in Nb_2O_5 [**31**].

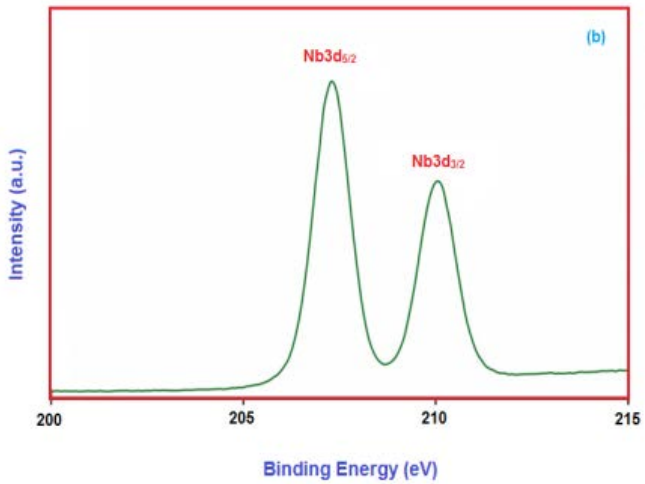

Figure 3.2(b) The XPS spectrum of Nb3d peaks of the Nb_2O_5 calcined at 450˚C.

3.3 Raman Spectra

Figure 3.3 shows the Raman spectra of sample Nb_2O_5 obtained by modified hydrothermal method and calcined at 450˚C. The spectra in Figure 3.3, corresponds to a well-developed crystalline structure of Nb_2O_5.For Irena *et al.* [**29**] the bands in the 400-800 cm^{-1} wavenumber region are assigned to the symmetric and antisymmetric stretching mode of the Nb-O-Nb linkage. While the Raman band at 235 cm^{-1} becomes the bending mode of Nb-O-Nb. The figure shows that the calcination temperature of 450°C is ideal for obtaining the crystalline Nb_2O_5. In general the Raman study shows that an increase of the synthesis temperature causes an increase in the material crystallinity because an increase in the synthesis temperature led to a sharp peak, this fact is verified with the values of the crystallite size that were estimated by the Scherrer equation (Table 3.1).

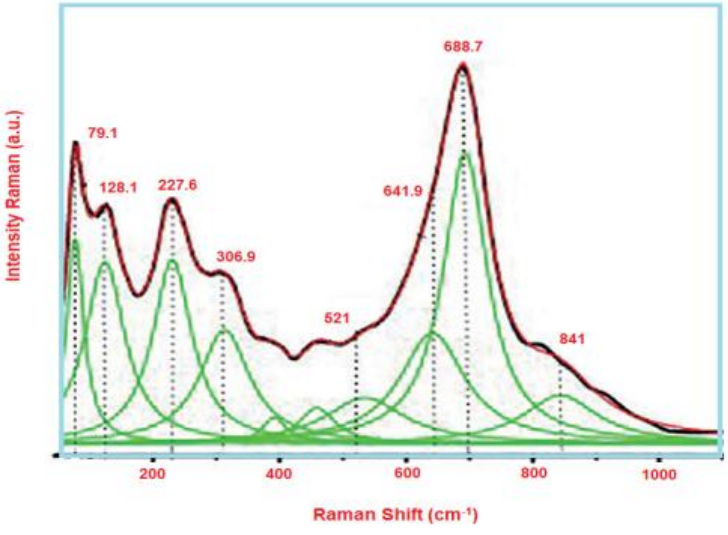

Figure 3.3 Raman spectra for sample Nb-450 calcined at 450˚C.

3.4 FTIR Analysis

Figure 3.4 displays the FTIR spectra of the samples Nb-400, Nb-450 and Nb-500. After calcination at 400˚C, an intense broad band centered around 659 cm^{-1} and a shoulder-like band near 988 cm^{-1} are observed. The increase of the calcination temperature brings about an increase in intensity of the bands. The intensity of Nb-400 sample is lower as compared to that of Nb-450 and Nb-500 samples that was due to the amorphous nature at that temperature, and was

in agreement with the XRD pattern. While increasing calcination temperature leads to an increase in the intensity of bands. This is probably because of the greater asymmetry in the unit cell and the possible interaction between the Nb–O groups. The band near 988 cm^{-1} appears in all the spectra, which has been assigned to a highly distorted octahedral NbO_6 containing Nb=O bond. An increase in the calcination temperature leads to an increase in the intensity of the Nb=O bonds [**30**]. Also, the relative intensity of the band at the lower frequency of near 649 cm^{-1}, which is assigned to the Nb–O bond of the slightly distorted NbO_6 octahedra, is increased with an increase in the temperature. The increase in the intensity of the bands at 659 and 988 cm^{-1} in high calcination temperatures may be due to the existence of more Nb–O and Nb=O bonds in the structure adopted at 450˚C, respectively.

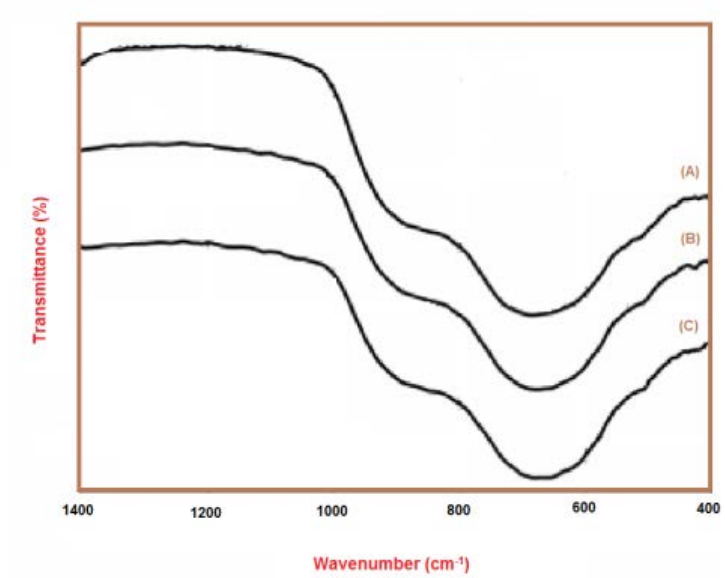

Figure 3.4 FTIR spectra of (A) Nb-400, (B) Nb-450 and (C) Nb-500 samples.

3.5 Scanning Electron Microscopy (SEM)

Figure 3.5 shows the SEM images, displaying the morphologies of the Nb_2O_5 particles obtained by calcination at 450˚C. As shown in Figure, the Nb_2O_5 sample has a spongy tissue with small particles (<10 nm). This tissue possesses the highest surface area (75.42m^2/g) and a uniform distribution of pores. However, it was observed that with increasing the calcination temperature leads to a strongly agglomeration in case of Nb-500 and Nb-550 samples (SEM images are not presented here).

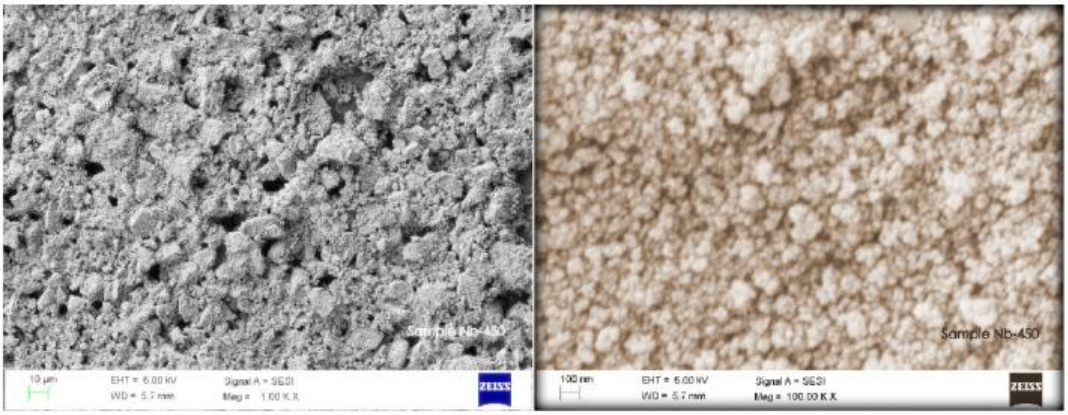

Figure 3.5 SEM images of sample Nb-450 calcined at 450˚C.

3.6 Determination of Film Thickness

To measure the effect of film thickness, the screen printing of the sample Nb-450 was done in three different cycles (Table 3.2). The film thickness was measured by a weight difference method [**15**] in which weight of the sample, area and densities were considered. In order to measure the thickness of the thin films by using weight difference method, error and accuracy was found to be ± 5 % nm. The relation of the film thickness (t) with sample weight (M (in g)), density of material (ρ (in gcm^{-3})) and sample area (A (in cm^2)) is presented in the following equation:

$$t = \frac{M}{A\rho}$$

The thickness of the film was in the range of 100-130 nm. The values of the film thickness with printing cycle are given in Table 3.2.

Table 3.2 Details of samples with film thickness and activation energy.

Sample	Screen Printing Cycle	Film Thickness (nm)	Activation Energy (ΔE)	
			At 30˚C	At 100˚C
Nb-450-I	05	100	0.42 eV	0.57 eV
Nb-450-II	10	122	0.34 eV	0.41 eV
Nb-450-III	15	130	0.22 eV	0.31 eV

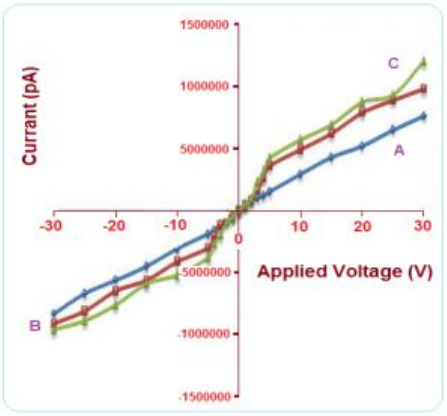

Figure 3.6 I–V characteristics of thin films (A) Nb-450-I, (B) Nb-450-II and (C) Nb-450-III.

3.7 I-V Characteristics

The sensor films were prepared in dimension as: 1.5 cm × 1 cm. The contacts were made by silver paste on thin film surface. Figure 3.6 shows the I–V characteristics of samples Nb-450-I, Nb-450-II and Nb-450-III observed to be nearly symmetrical in nature indicating ohmic contacts. The non-linear I–V characteristics may be due to semiconducting nature of the films. Sample Nb-450-I, Nb-450-II and Nb-450-III are the films obtained by screen printing cycle intervals of: 5, 10 and 15 respectively. Therefore, the thickness of the films goes on increasing in the sequence of Nb-450-I > Nb-450-II > Nb-450-III.

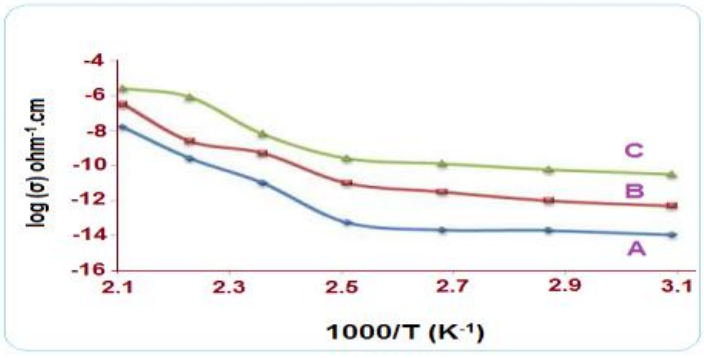

Figure 3.7 Variation of log (σ) with operating temperature (˚C) thin films (A) Nb-450-I, (B) Nb-450-II and (C) Nb-450-III.

3.8 Electrical Conductivity

Figure 3.7 show the variation of log (σ) with operating temperature. The conductivity of each sample is observed to be increasing with an increase in temperature range between 50˚C and 150˚C. The increase in conductivity with increase in temperature could be attributed to negative temperature coefficient of resistance and semiconducting

nature of nanostructured Nb_2O_5. For the metal oxide semiconductor thin films it is reported that, when thickness of the film increases activation energy goes on deceases [16, 17]. The activation energy calculated from slopes of line for sample Nb-450-I, Nb-450-II and Nb-450-III are given in Table 3.2. It is clear from Table 3.2 that, as film thickness of the sample goes on increasing; while the activation energy goes on decreasing. The decrease in activation energy with increasing film thickness may be due to the change in structural parameters, improvement in crystallite and grain size [18].

3.9 Gas Sensitivity Measurements

To investigate the gas sensing properties of the synthesized Nb_2O_5 thin films, various gases acetone, ammonia and LPG were selected. We also have repeated testing for at least two sensors for each nanostructure and sensing test condition, which makes the results more reliable and repeatable. All the gas sensing measurements were done at the temperature range from 50 to 300˚C.

3.9.1 Effect of Operating Temperature

Figure 3.8 shows the variation in response with the operating temperature to 400 ppm of acetone, ammonia and LPG gases for Nb-450-II thin films for 10 min. For all the gases, the response increases with increase in operating temperature and reach maximum at 250˚C for NH_3 gas. Gas sensitivity depends on two factors, namely: the speed of chemical reaction on the surface of the grains and the speed of the diffusion of gas molecules to that surface. At low temperatures the sensor response is restricted by the speed of chemical reactions. At higher temperature the sensor response is restricted by the speed of the diffusion of gas molecules to the sensor surface.

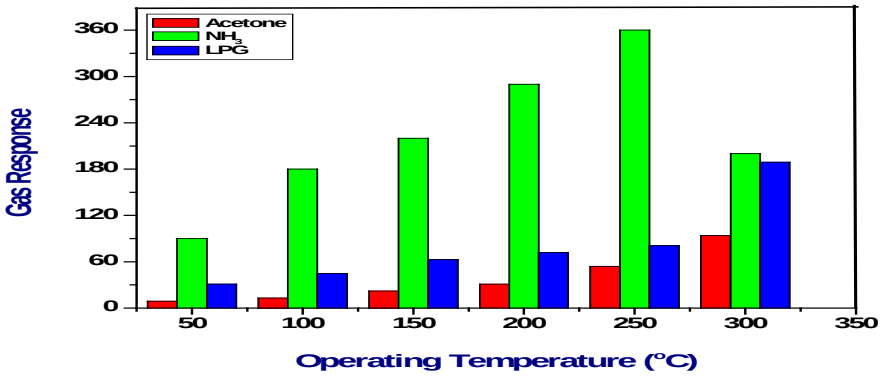

Figure 3.8 Gas response of Nb-450-II for 400 ppm of various gases.

[Gas Concentration: 400 ppm, Gas Exposure time: 10 min.]

At some intermediate temperature the rate of two processes; the chemical reaction on the surface of the grains and the diffusion of gas molecules on sensor surface become equal, at that point the sensor response reaches its maximum. According to this mechanism for every gas there is a specific temperature at which the sensor response attains its highest value which depends upon the nature of sensor and interacting gas. A 40-min response time is not long enough to obtain a stable response at low temperature 250˚C. Nevertheless, any bulk effect is unlikely because of the rapid desorption observed. For many oxides, such as SnO_2, TiO_2 and Nb_2O_5, bulk properties are thermodynamically equilibrated with oxygen partial pressure only at the working temperature above 700°C [7].

At lower temperatures, the conductivity variation is associated to a surface conductivity variation. *Heiland* reported that, in *n*-type semiconductor, chemisorption of oxidizing or reducing gases induces the creation of acceptor or donor surface states, respectively [8]. The presence of a reducing gas creates surface states located above the Fermi level and sets up a charge enhancement zone at the grain surface. This phenomenon is the more important as the concentration of the reducing gas NH_3 increases [9].

3.9.2 Effect of Gas Concentration

Figure 3.9 shows the relation between gas response and concentration of various test gas for Nb-450-II sample at 250°C. From the graph, it was observed that the sensitivity of thin films for all test gas increases linearly with increase in gas concentration up to 1000 ppm. Beyond 400 ppm the increase in sensitivity is slow and it almost

saturates at 1000 ppm. At a low concentration of gas, when exposed on a fixed surface area of a sample, there is a less coverage by gas molecules on the surface and hence slow surface reaction occurs. An increase in gas concentration increases the surface reaction due to a larger surface coverage. A further increase in surface reaction will be gradual when the saturation point on the coverage by molecules is reached.

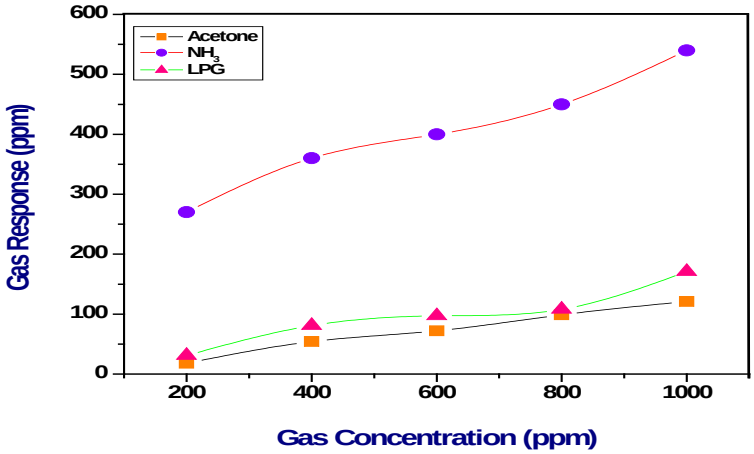

Figure 3.9 Gas response of Nb-450-II for various gases.
[Operation Temperature: 250˚C, Gas Exposure time: 10 min.].

3.9.3 Effect of Calcination Temperature

The effect of calcination temperature on gas sensing property of screen printed Nb_2O_5 thin film sensors as investigated and results are presented in Figure 3.10. Figure 3.10 depicts that, the Nb_2O_5 ample obtained at 450˚C showed maximum sensitivity for 400 ppm of ammonia at 250˚C. This is because of the smaller crystallite size (11.7 nm) and the large specific surface area (75.42m^2/g) of the Nb-450-II. From Table 3.1, it is clear that, the crystallite size of as synthesized Nb_2O_5 sensors increases with calcination temperature. Moreover, the specific surface area decreases on calcination of the samples above 450˚C. Decreased specific surface area (in Nb-500-II and Nb-550-II thin films) provides less number of available sites for adsorption of target gas that in turn decreases the sensing activity of the sensors.

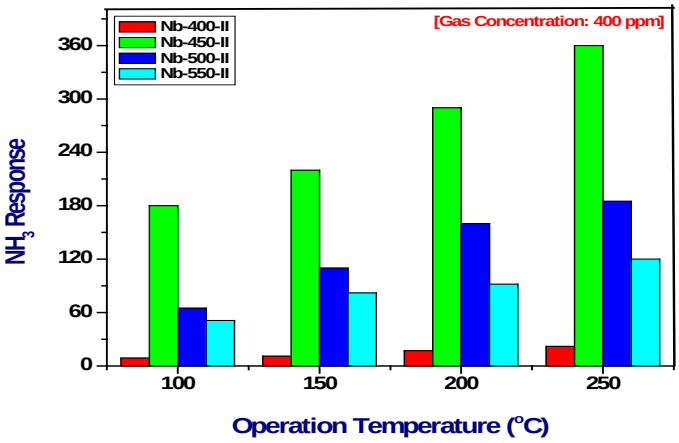

Figure 3.10 Effect of calcination temperature on ammonia (400 ppm) sensing efficiency of screen printed Nb_2O_5 thin films.

3.9.4 Response and Recovery Time

The transient response characteristics of Nb-450-I, Nb-450-II and Nb-450-III exposed to 1000 ppm towards ammonia are shown in Figure 3.11. From figure it is observed that, the films exhibited enhanced sensitivity towards Nb-450-II and is mainly attributed to the change in morphology of the sample with increase in thickness of the film

significantly. The adsorption of oxygen on the surface increases the resistance of the sensor material due to transport of electrons from conduction band to adsorbed oxygen which results in increase in gas response. The response and recovery time values for the samples are given in Table 3.3. Fast response of 90 sec was observed in case of Nb-450-II, which is attributed to small crystallite size and subsequently large surface area. From the results, we concluded that for Nb-450 thin films thickness of 122 nm is an appropriate value for its use in gas sensing applications. The Nb-450-II thin film sensor attains its initial value within 220 sec. which indicates that its surface rejuvenates after refreshing with air. The short response and recovery times are the merit of the Nb-450-II sample.

Table 3.3 Response and recovery time for Nb-450 thin film sensors.

Time (sec)	Nb-450-I	Nb-450-II	Nb-450-III
$t_{(response)}$	120	90	135
$t_{(recovery)}$	435	220	558

3.9.5 Stability

The sensor reliability was strongly dependent on the stability exhibited by the sensor material. It was well known that oxide based sensor possess common drawback of decrease in response due to ageing induced effects. Stability is the consistence of the response of a sensor under continuous testing. The responses of the Nb-450-II thin film sensor towards ammonia were measured on 20th, 40th and 60th days after the first measurement and are shown in Figure 3.12. It was found that after two months, the material performs 92% of it was earlier performance confirming the stability.

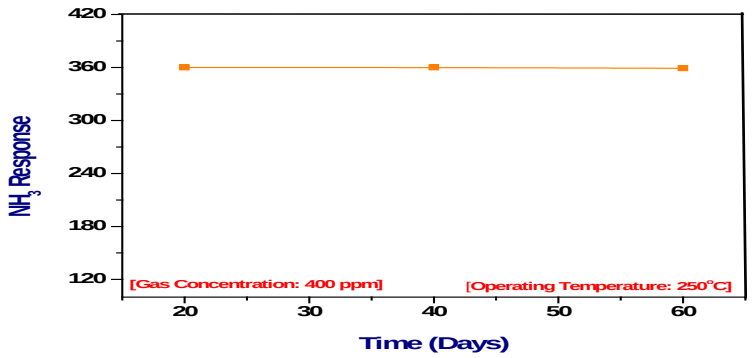

Figure 3.11 Plot of stability for Nb-450-II sample.

4. Conclusion

The nanocrystalline Nb_2O_5 sensors with high surface area (up to 75.42m^2/g) and smaller crystallite size were prepared by modified hydrothermal method. The gas sensing performance of Nb_2O_5 sensors was demonstrated for acetone, ammonia and LPG. It was found that, Nb-450 thin films show the fast and optimum response towards 400 ppm ammonia gas at 250˚C. For the recovery process, the sample indicated slow recovery performance under most sensing situations. However, a comparatively better performance is observed over most of the reported Nb_2O_5 based sensors. To further improve the performance and to find better selectivity for other gases such as H_2S, the Nb_2O_5 samples are further modifications are in progress.

References

[1] Y.D. Wang, L.F. Yang, Z.L. Zhou, Y.F. Li, X.H. Wu, “Effects of calcining temperature on lattice constants and gas-sensing properties of Nb_2O_5”, *Materials Letters*, 49(5) (**2001**) 277-281.
[2] S.H. Mujawar, A.I. Inamdar Patil, S.B. Patil, P.S. Patil, “Electrochromic properties of spray-deposited niobium oxide thin films”, *Solid State Ionics*, 177 (37-38) (**2006**) 3333-3338.
[3] R. Jose, V. Thavasi, S. Ramakhrisna, “Metal Oxides for Dye Sensitized Solar Cells”, *Journal of the American Ceramic Society*, 92(2) (**2009**) 289-301.
[4] M. Lira-Cantu, F.C. Krebs, “Hybrid solar cells based on MEHPPV and thin film semiconductor oxides (TiO_2, Nb_2O_5 , ZnO, CeO_2 and CeO_2 –$CTiO_2$) Performance improvement during long-time irradiation”, *Solar Energy Materials and Solar Cells*, 90(14) (**2006**) 2076-2086.

[5] K. S. Ahn, M. S. Kang, J. K. Lee, B. C. Shin, J. W. Lee, "Enhanced electron diffusion length of mesoporous TiO_2 film by using Nb_2O_5 energy barrier for dye-sensitized solar cells", *Applied Physics Letters*, 89(1) (**2006**) 013103.
[6] P. Carniti, A. Gervasini, M. Marzo, "Dispersed NbO_x Catalytic Phases in Silica Matrixes: Influence of Niobium Concentration and Preparative Route", *The Journal of Physical Chemistry C*, 112(36) (**2008**) 14064-14074.
[8] T. Sreethawong, S. Ngamsinlapasathian, S. H. Lim, S. Yoshikawa. "Investigation of thermal treatment effect on physicochemical and photocatalytic H_2 production properties of mesoporous-assembled Nb_2O_5 nanoparticles synthesized via a surfactant-modified sol–gel method", *Chemical Engineering Journal*, 215- 216 (**2013**) 322-330.
[9] M. L. Marin, G. L. Hallett-Tapley, S. Impellizzeri, C. Fasciani, S. Simoncelli, J.C. Netto-Ferreira, J.C.Scalano, "Synthesis, acid properties and catalysis by niobium oxide nanostructured matrrials", *Catalysis Science & Technology*, 9(4) (**2014**) 3044-3052.
[10] G. Shen, P.C. Chen, K. Ryu, C. Zhou, "Devices and chemical sensing applications of metal oxide nanowires", *Journal of Materials Chemistry*, 19(7) (**2009**) 828-839.
[11] N. S. Harale, D. L. Kamble, M. G. Gang, V. K. Rao, J. H. Kim, P. S. Patil, "Exotic fern-like morphologies", *Materials Today*, 16 (11) (**2013**) 452-453.
[12] D. Rosenfeld, P. E. Schmid, S. Széles, F. Lévy, V. Demarne, and A. Grisel, "Electrical transport properties of thin-film metal-oxide-metal Nb_2O_5 oxygen sensors", *Sens. Actuators B*, 37(1-2) (**1996**) 83-89.
[13] L. Chambon, C. Maleysson, A. Pauly, J. P. Germain, V. Demarne, and A. Grisel, "Investigation, for NH_3 gas sensing applications, of the Nb_2O_5 semiconducting oxide in the presence of interferent species such as oxygen and humidity", *Sens. Actuators B*, 45(2) (**1997**) 107-114.
[14] L. Chambon, A. Pauly, J. P. Germain, C. Maleysson, V. Demarne, A. Grisel, "A model for the responses of Nb_2O_5 sensors to CO and NH_3 gases", *Sens. Actuators B*, 43 (1-3) (**1997**) 60-64.
[15] Z. Wang, Y. Hu, W. Wang, X. Zhang, B. Wang, H. Tian, Y. Wang, J. Guan, H. Gu "Fast and highly-sensitive hydrogen sensing of Nb_2O_5 nanowires at room temperature", *Int. J. Hydrogen Energy* , 37(5) (**2012**) 4526- 4532.
[16] T. Hyodo, J. Ohoka, Y. Shimizu, M. Egashira, "Design of anodically oxidized Nb_2O_5 films as a diode-type H_2 sensing material", *Sens. Actuators B*, 117(2) (**2006**) 359-366.
[17] L. Chevallier, E. D. Bartolomeo, M. L. Grilli, M. Mainas, B. White, E. D. Wachsman, E. Traversa, "Non-Nernstian planar sensors based on YSZ with a Nb_2O_5 electrode", *Sensors and Actuators B Chemical*, 129(2) (**2008**) 591-598.
[18] L. Chevallier, E. Di Bartolomeo, M. L. Grilli, E. Traversa, "High temperature detection of CO/HCs gases by non-Nernstian planar sensors using Nb_2O_5 electrode", *Sensors and Actuators B Chemical*, 130 (1) (**2008**) 514-519.
[19] H. G. Moon, H. W. Jang, J. S. Kim, H. H. Park, S. J. Yoon, "A route to high sensitivity and rapid response Nb_2O_5 -based gas sensors: TiO_2 doping, surface embossing, and voltage optimization", *Sens. Actuators B Chemical*, 153(1) (**2011**) 37-43.
[20] T. Hyodo, H. Shibata, Y. Shimizu, M. Egashira, "H_2 sensing properties of diode-type gas sensors fabricated with Ti- and/or Nb-based materials", *Sens. Actuators B Chemical*, 142(1) (**2009**) 97-104.
[21] A. Kohli, C. C. Wang, S. A. Akbar, "Niobium pentoxide as a lean-range oxygen sensor", *Sens. Actuators B Chemical*, 56(1-2) (**1999**) 121-128.
[22] L. Chevallier, E. Traversa, E. D. Bartolomeo, "Propene detection at high temperatures using highly sensitive non-Nernstian electrochemical sensors based on N_b and T_a Oxides", *Journal of The Electrochemical Society*, 157(11) (**2010**) J386-J391.
[23] M. Suzana, P. Francisco, W. S. Cardoso, Y. Gushikem, "Carbon paste electrodes of the mixed oxide SiO_2/Nb_2O_5 prepared by the sol–gel method: dissolved dioxygen sensor", *Journal of Electroanalytical Chemistry*, 574(2) (**2005**) 291-297.
[24] U. Cvelbar, K. Ostrikov, A. Drenik, M. Mozetic, "Nanowire sensor response to reactive gas environment", *Appl. Phys. Letters*, 92(13) (**2008**) 133505(1) -133505(3).
[25] K. Kato, S.Tamura, "Die Kristallstruktur von T-Nb_2O_5", *Acta Crystallographica Section B*, B31 (**1975**) 673-677.
[26] Ikeya T, Senna M, "Change in the structure of niobium pentoxide due to mechanical and thermal treatments", *Journal of Non- Crystalline Solids*, 105(3) (1988) 243-250.
[27] S. Ge, H. Jia, H. Zhao, Z. Zheng, L. Zhang, "First observation of visible light photo-catalytic activity of carbon modified Nb_2O_5 nanostructures", *Journal of Materials Chemistry*, 20(15) (**2010**) 3052–3058.
[28] D. Regonini, A. Jaroenworaluck, R. Stevens, C.R. Bowen, "Effect of heat treat-ment on the properties and structure of TiO_2 nanotubes phase composition and chemical composition", *Surface and Interface Analysis*, 42 (3) (**2010**) 139– 144.
[29] J.Z. Ou, R.A. Rani, M. H. Ham, M. R. Field, Y. Zhang, H. Zheng, P. Reece, S. Zhuiykov, S. Sriram, M. Bhaskaran, R.B. Kaner, K. K. Zadeh, "Elevated temperature anodized Nb_2O_5: a photoanode material with exceptionally large photo conversion efficiencies", *ACS Nano*, 6(5) (**2012**) 4045–4053.
[30] I. Mickova, "Photoelectrochemical Study of Anodically Formed Oxide Films on Niobium Surfaces", *Croatica*

Chemica Acta, 83(2) (**2010**) 113-120.
[31] S. M. Maurer and E. I. Ko, "Structural and acidic characterization of niobia aerogels", *J. Catalysis*, 135 (1) (**1992**) 125–134.
[32] V. B. Patil, G. S. Shahane and L. P. Deshmukh, "Studies on photoelectrochemical (PEC) cells; A correlation between electrochemical and material properties", *Materials Chemistry and Physics*, 80(3) (**2003**) 625-632.
[33] R. H. Bari, S. B. Patil, P. P. Patil, A. R. Bari, "Detection of H_2S gas at lower operating temperature using sprayed nanostructured In_2O_3 thin films", *Bulletin of Material Science*, 36(6) (**2013**) 967–972.
[34] R. H. Bari, S. B. Patil, A. R. Bari, "Influence of precursor concentration solution on CO sensing performance of sprayed nanocrystalline SnO_2 thin films", *Optoelectronics and advanced materials rapid communication*, 6(9) (**2012**) 887-895.
[35] R. B. Kale, C. D. Lokhande, "Band gap shift, structural characterization and phase transformation of CdSe thin films from nanocrystalline cubic to nanorod hexagonal on air annealing", *Semiconductor Science Technology*, 20(1) (**2005**) 1-7.
[36] D.E. Williams, "Conduction and gas response of semiconductor gas sensors, in: P.T. Moseley, B.C. Tofield (Eds.), *Solid Gas Sensors, Adam Hilger, Bristol*, **1987**.
[37] G. Heiland, "Homogeneous semiconducting gas sensors", *Sensors and Actuators*, 2 (**1982**) 343–361.
[38] J.A. Rodriguez, C.T. Campbell, "A quantum-chemical study of the chemisorption of ammonia, pyridine, formaldehyde, formate and methoxy of ZnO (0001)", *Surface. Sci.* 194(3) (**1988**) 475–504.